

ABSENCE OF REFLECTION FEATURES IN *NuSTAR* SPECTRA OF THE LUMINOUS NEUTRON STAR
X-RAY BINARY GX 5–1

JEROEN HOMAN,^{1,2,3} JAMES F. STEINER,^{3,4} DACHENG LIN,⁵ JOEL K. FRIDRIKSSON,⁶ RONALD A. REMILLARD,³
JON M. MILLER,⁷ AND RENEE M. LUDLAM⁷

¹*Eureka Scientific, Inc., 2452 Delmer Street, Oakland, CA 94602, USA*

²*SRON, Netherlands Institute for Space Research, Sorbonnelaan 2, 3584 CA Utrecht, The Netherlands*

³*MIT Kavli Institute for Astrophysics and Space Research, 70 Vassar Street, Cambridge, MA 02139, USA*

⁴*Einstein Fellow*

⁵*Space Science Center, University of New Hampshire, Durham, NH 03824, USA*

⁶*Anton Pannekoek Institute, University of Amsterdam, Science Park 904, 1098 XH, Amsterdam, The Netherlands*

⁷*Department of Astronomy, University of Michigan, 1085 South University Ave, Ann Arbor, MI 48109-1107, USA*

ABSTRACT

We present *NuSTAR* observations of the luminous neutron star low-mass X-ray binary (NS LMXB) and Z source GX 5–1. During our three observations made with separations of roughly two days, the source traced out an almost complete Z track. We extract spectra from the various branches and fit them with a continuum model that has been successfully applied to other Z sources. Surprisingly, and unlike most of the (luminous) NS-LMXBs observed with *NuSTAR*, we do not find evidence for reflection features in any of the spectra of GX 5–1. We discuss several possible explanations for the absence of reflection features. Based on a comparison with other accreting neutron star systems and given the high luminosity of GX 5–1 (~ 1.6 – 2.3 times the Eddington luminosity, for a distance of 9 kpc), we consider a highly ionized disk the most likely explanation for the absence of reflection features in GX 5–1.

Keywords: accretion, accretion disks — stars: neutron — X-rays: binaries — X-rays: individual (GX 5–1)

arXiv:1711.07263v2 [astro-ph.HE] 26 Jun 2018

1. INTRODUCTION

The most luminous neutron star low-mass X-ray binaries (NS-LMXBs), the so-called Z sources, trace out characteristic multi-branched tracks in their X-ray color-color and hardness-intensity diagrams (HIDs). The origin of these branches remains poorly understood, but given the high luminosity of the Z sources — near or above the Eddington luminosity (L_{Edd}) — radiation pressure is believed to play an important role (Church et al. 2006; Lin et al. 2009). Based on the shape of their tracks, two subclasses of the Z sources are generally recognized: the Sco-like and the Cyg-like Z sources (Kuulkers et al. 1994). From transient and highly variable sources, we know that Cyg-like Z-source behavior is associated with higher luminosities (Homan et al. 2010; Fridriksson et al. 2015).

Various models have been proposed to fit the continuum spectra of the Z sources (e.g. Church et al. 2006; Lin et al. 2009; Titarchuk et al. 2014). While most provide statistically acceptable fits, they often result in different interpretations of Z-source behavior (e.g. evolution of the inner disk radius, boundary layer area, and mass accretion rate). Reflection features in the X-ray spectra (e.g., Ross et al. 1999) could shed additional light on the changes in the accretion flow along the Z track. They are the result of irradiation of the inner accretion disk and are sensitive to changes in the accretion geometry. In black hole (BH) X-ray binaries and low-luminosity NS-LMXBs the irradiating flux is supplied by a hot corona (e.g., Fürst et al. 2015; Sleator et al. 2016; Wang et al. 2017), while in the high-luminosity NS-LMXBs, the boundary layer is the main contributor (e.g., Miller et al. 2013; Ludlam et al. 2017c).

The reflection process results in two main spectral features (Ross et al. 1999): an Fe K_{α} line around 6.4–7.0 keV (due to fluorescence) and (less frequently) a broad hump between 10–30 keV (due to Compton backscattering). Modeling of these features can provide valuable information on the geometry of the accretion flow (Fabian & Ross 2010) and changes therein. The relativistically broadened Fe K_{α} line, in particular, is frequently used to measure inner disk radii, in order to determine black hole spins (see Reynolds 2014, for a review) or constrain the neutron star equation of state (e.g., Cackett et al. 2008, 2010). In view of the uncertainties in modeling the Z-source spectra, the Fe K_{α} line is also valuable in that it could provide independent constraints on the disk and boundary layer.

NuSTAR observations of 13 NS-LMXBs have been published, including two Sco-like Z sources (GX 17+2 and GX 349+2; Ludlam et al. 2017c; Coughenour et al. 2017) and one Cyg-like one (Cyg X-2; Mondal et al.

2018). As can be seen from Table 1, Fe K_{α} lines were found in 11 of these sources. Here, we present an analysis of three *NuSTAR* observations of GX 5–1, a Cyg-like Z source (Kuulkers et al. 1994). The aim of these observations was to use inner disk measurements obtained from the reflection component as a check for the inner disk behavior obtained from our continuum modeling (see Coughenour et al. 2017 and Mondal et al. 2018, for similar attempts). However, no reflection features were detected in the spectra of GX 5–1. In Section 2, we present our observations and data analysis; in Section 3, the results of our analysis; and in Section 4 we discuss possible explanations for the absence of reflection features in GX 5–1.

2. OBSERVATIONS AND DATA ANALYSIS

2.1. *NuSTAR*

GX 5–1 was observed three times with *NuSTAR*: on 2016 April 9, 11, and 13 (ObsIDs 30102056002, 30102056004, and 30102056006). The observations had dead-time-corrected exposures of 10.3–11.2 ks. The reason for spacing the observations ~ 2 days apart was to increase the chances of covering as much of the Z track as possible with relatively short observations. The data were analyzed with the NuSTARDAS subpackage of HEASOFT V6.19, using calibration files from 2016 December. Each observation was reprocessed with *nupipeline*. Source spectra and light curves were extracted from the FPMA/FPMB detectors using a circular region with a $120''$ radius, centered on the source. For background spectra and light curves, a similar extraction region was used, located $\sim 8'-9'$ away from the source.

To construct a HID, we used *nuproducts* to extract source/background light curves with time bins of 100 s in two energy bands: 5.6–9.6 keV and 9.6–20 keV. Live-time, point-spread-function, exposure, and vignetting corrections were applied. Background-corrected light curves from FPMA and FPMB were added, and the resulting light curves for the two bands were summed to produce a broadband light curve that is used as the intensity in the HID. The ratio of the second and first energy bands was used as the hardness.

Because the source showed strong evolution in its HID, spectra were extracted based on location along the Z track to minimize the effects of mixing different spectral shapes. Parts of the HID were selected manually and appropriate good-time intervals were produced for each selection. Spectra were extracted with *nuproducts* using these good-time intervals. The FPMA/FPMB spectra were fitted simultaneously, and a constant (with fitted values between 0.97 and 0.98) was introduced in

Table 1. Neutron star LMXBs observed with *NuSTAR*

Source	L/L_{Edd}^a	Fe K_α line?	References
Cen X-4	3.8×10^{-6}	no	Chakrabarty et al. (2014)
4U 1608–52	0.01–0.02	yes	Degenaar et al. (2015)
4U 1636–536	0.01, 0.03–0.06	yes	Ludlam et al. (2017c), Wang et al. (2017)
1RXS J180408.9–34205	0.03–0.04, 0.1	yes	Degenaar et al. (2016), Ludlam et al. (2016)
XTE J1709–267	0.04–0.06	yes	Ludlam et al. (2017a)
4U 1728–34	0.08, 0.06–0.09	yes	Sleator et al. (2016), Mondal et al. (2017)
GS 1826–238	0.13	no	Chenevez et al. (2016)
4U 1705–440	0.2	yes	Ludlam et al. (2017c)
Ser X-1	0.6	yes	Miller et al. (2013), Matranga et al. (2017)
Aql X-1	0.14–0.7	yes	King et al. (2016), Ludlam et al. (2017b)
GX 349+2	0.4–0.7 ^b	yes	Coughenour et al. (2017)
GX 17+2	1.2	yes	Ludlam et al. (2017c)
Sco X-1	1.3	yes	This work
Cyg X-2	1.8 ^c	yes	This work, Mondal et al. (2018)
GX 5–1	1.6–2.3	no	This work

^a L_{Edd} defined as 1.8×10^{38} erg s⁻¹.

^b Assuming 5 kpc (Christian & Swank 1997).

^c Assuming 11 kpc (Galloway et al. 2008).

our models to account for cross-calibration differences. Spectral channels below 3 keV and above 50 keV were excluded and the remaining channels were grouped to a minimum of 30 counts per spectral bin. Spectral fits were made with XSPEC V12.9.1 (Arnaud 1996). The errors quoted in this paper are all 1σ .

Swift observations made quasi-simultaneously with our first and second observations suffered from strong pile-up and a soft excess below 1 keV that is commonly seen in heavily absorbed sources. Due to problems in cross-calibration with the *NuSTAR* spectra, the *Swift* spectra were not included in our analysis.

3. RESULTS

3.1. Hardness-Intensity Diagram

In Figure 1 we show the combined HID of our three *NuSTAR* observations of GX 5–1. An almost complete Z track was traced out. We have labeled and colored the various Z-source branches. During the first observation, the source traced out the flaring branch (FB), the “dipping” FB, and the lower part of the normal branch (NB). The full NB was traced out during the second observation, while the upper NB and the horizontal branch (HB) were traced out during the third observa-

tion. Gaps in the track, most notable on the “dipping” FB and the HB, are the result of Earth occultations and passages through the South Atlantic Anomaly.

3.2. Spectra

FPMA/FPMB spectra were extracted from five locations along the Z track in the HID, corresponding to the black and red colored regions in Figure 1. We note that spectra for the lower NB were only extracted from observation 1 and upper NB spectra only from observation 2, even though these parts of the Z track were also partially traced out in other observations.

Following Lin et al. (2009), we started by fitting the spectra with a continuum model consisting of a multi-color disk blackbody (`diskbb` in XSPEC) and a blackbody (`bbodyrad`). We used the `tbnewfeo` model (Wilms et al. 2000) for interstellar absorption, with the abundances set to `wilm` and cross sections set to `vern` (Verner et al. 1996). The values of N_{H} were left free for each selection. Although this model generally provided good fits to the continua below ~ 15 – 25 keV, strong positive residuals were seen above that energy, while negative residuals around 7 keV were seen in some spectra as well (see Fig. 2, middle panel). This model resulted in

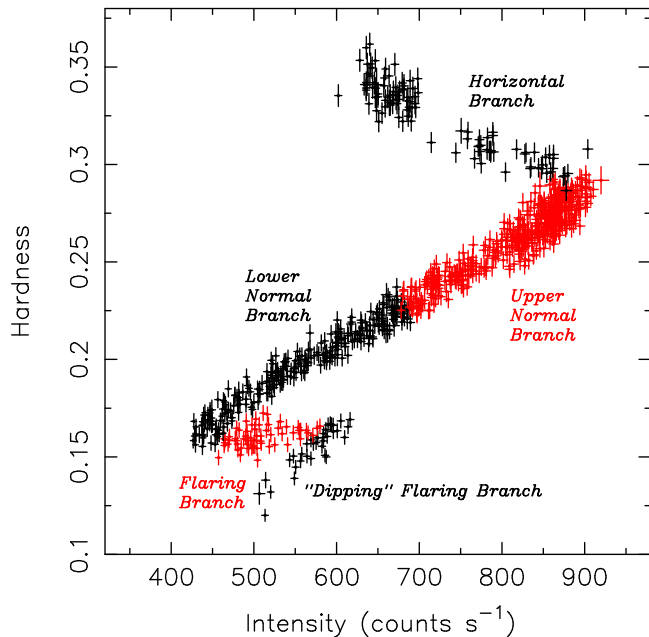


Figure 1. Combined *NuSTAR* HID of GX 5–1. The various Z-source branches are labeled and colored black/red to distinguish selections used for spectral analyses. Data point represent 100 s time intervals.

$\chi_{\text{red}}^2/d.o.f. = 1.39/4698$. The addition of a power-law component (`pegpwlw`), as clearly detected in *INTEGRAL* spectra of GX 5–1 (Paizis et al. 2005), improved the high-energy residuals, as well as those around 7 keV, and resulted in $\chi_{\text{red}}^2/d.o.f. = 1.15/4693$. However, the power-law indices were very high, increasing from 3.6 on the HB to 4.5 on the FB, before sharply dropping to 2.1 on the dipping FB. Such steep power laws can result in degeneracies between N_{H} , the `diskbb` parameters, and the power-law index. To lessen these degeneracies, we replaced the power law with a cutoff power law (`cutoffpl`). We additionally tied the power-law index between all observations, but left the cutoff energy to vary. We also tied the N_{H} values between the spectra, as it was otherwise found to increase substantially on the FB and dipping FB. Although these constraints did not significantly improve the fit ($\chi_{\text{red}}^2/d.o.f. = 1.14/4697$), the resulting power-law index was considerably lower: 3.02 ± 0.12 . Physically motivated Comptonization models, such as, e.g., `nthcomp` (Zdziarski et al. 1996; Życki et al. 1999), did not provide better fits than our model with the cutoff power law, nor did they solve the issues with the high power-law indices. An example fit with our final model to the HB spectra is shown in Figure 2.

In Table 2 we report the fit results with our final model. Some general trends can be seen: as the source moves from the HB to the dipping FB the temperatures of the disk and blackbody (kT_{disk} and kT_{bb} , re-

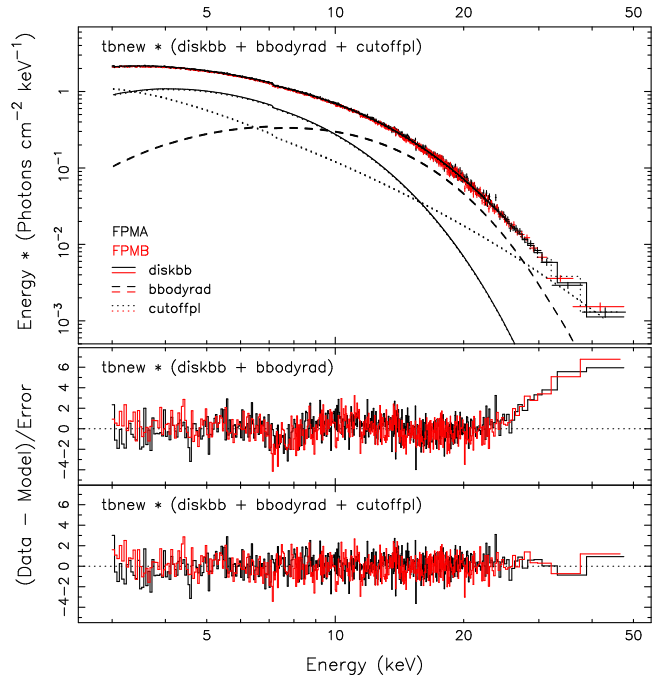


Figure 2. Fit to the HB spectra with our final model (top), and residuals from fits with our final model (bottom) and a model without a cutoff power law (middle).

spectively) decrease monotonically, while their radii increase (quite dramatically so on the FB and dipping FB). The power-law contribution to the 3–50 keV flux shows an overall decrease along the Z track, while the cutoff shows a moderate decrease in energy (E_{cut}); it was poorly constrained on the dipping FB and fixed to the FB value. The broadband unabsorbed luminosity (L_{1-100}), obtained by extrapolating¹ the model fits down to 1 keV and up to 100 keV and assuming a distance of 9 kpc ($d_9=1$), varies between $\sim 3.0 \times 10^{38}$ erg s⁻¹ and $\sim 4.3 \times 10^{38}$ erg s⁻¹, peaking toward the upper NB. For a $1.4 M_{\odot}$ neutron star, these luminosities correspond to Eddington ratios of $\sim 1.6\text{--}2.3(d_9)^2$.

The lack of coverage below 3 keV may lead to considerable (systematic) uncertainties in the continuum parameters, in particular the disk temperatures/radii, and the N_{H} values. One of the main goals of our observations was to use reflection features, as seen in other luminous NS-LMXBs, to obtain independent measures of the evolution of the inner disk radius along the Z track. However, we do not see any indications for an Fe K_{α} line or a Compton hump in our spectra of GX 5–1. To illustrate this, we followed Ludlam et al. (2017c) and excluded data in the 5.0–8.0 keV range in fits to the

¹ The power-law contribution was only measured in the 3–100 keV range

Table 2. Spectral-fit parameters for model `tbnew_feo × (diskbb + bbodyrad + cutoffpl)`

	HB	Upper NB	Lower NB	FB	Dipping FB
kT_{disk} (keV)	1.99±0.06	1.83±0.02	1.45±0.03	0.98±0.02	0.80±0.01
R_{in} (km)	8.1±0.5	12.4±0.4	17.8±0.7	38±3	70±3
kT_{bb} (keV)	2.51±0.04	2.46±0.03	1.89±0.03	1.480±0.007	1.425±0.003
R_{bb} (km)	4.1±0.3	3.7±0.2	6.5±0.4	16.7±0.3	22.8±0.2
E_{cut} (keV)	18±3	13.1±1.6	10.9±1.2	8.2±1.0	8.2 (fixed)
$F_{3-50 \text{ keV}}^{\text{a}}$ (10^{-8} erg cm $^{-2}$ s $^{-1}$)	2.12±0.02	2.46±0.01	1.80±0.01	1.70±0.01	1.85±0.01
PL Fraction (%)	29±5	23±5	26±6	15±5	1.1±1.4
$L_{1-100 \text{ keV}}$ (10^{38} erg s $^{-1}$)	2.98±0.01	3.85±0.02	3.15±0.02	3.44±0.02	4.25±0.02

NOTE—The best-fit N_{H} value and cutoff power-law index were $(6.20 \pm 0.16) \times 10^{22}$ atoms cm $^{-2}$ and 3.02 ± 0.12 , respectively. For R_{in} , R_{bb} , and L_{1-100} we assumed a distance of 9 kpc (Christian & Swank 1997). For R_{in} we additionally assumed an inclination of 60° . For $L_{1-100 \text{ keV}}$ the power-law contribution was only measured between 3 and 100 keV.

^a Unabsorbed

spectra of each individual HID selection. All parameters were left free and the cutoff power-law index and N_{H} were no longer tied between selections, to limit possible bias. In Figure 3 (panels (a)–(e)) we plot data-to-model ratios resulting from these fits, but with data from the 5.0–8.0 keV range included again to look for indications of (broad) Fe K_{α} lines. None of the spectra show positive residuals, which would indicate the presence of such lines. We do, however, see strong negative residuals in the FB and dipping FB spectra. Although negative residuals could indicate the presence of absorbing material in our line of sight (e.g. caused by a wind outflow), the width of the features (i.e., broader than typically seen for wind lines) might alternatively suggest that they result from shortcomings in our continuum model on those branches.

For comparison with GX 5–1, we analyzed *NuSTAR* data of two other Z sources: Sco X-1 (observation 30001040002) and Cyg X-2 (observation 30001141002, see also Mondal et al. (2018)). The same analysis steps were followed as for GX 5–1. In the HIDs of both sources, a clear NB could be identified; for Sco X-1, we extracted a spectrum from the full NB, while for Cyg X-2 we extracted a spectrum from the upper NB (as the lower part was relatively sparsely covered). These spectra had similar signal-to-noise ratios as those of GX 5–1, and we applied the same model and procedure as for GX 5–1 to study the residuals in the 5–8 keV range. The resulting data/model ratios are shown in Figures 3f and 3g and obvious broad positive residuals around 6.5 keV can be seen for Sco X-1 and Cyg X-2. In Table 3 we give the fit parameters to the spectra of Sco X-1

and Cyg X-2, with a Gaussian added to our model to account for the Fe K_{α} line. Note that for Sco X-1, we used a power law without a cutoff. The fit parameters for Sco X-1 and Cyg X-2 are comparable to those found for GX 5–1 on the upper and lower NB, except for the fact that the power-law contribution appears to be higher in GX 5–1, especially compared to Sco X-1.

When fitted with a simple Gaussian, the lines in Sco X-1 and Cyg X-2 have equivalent widths ~ 80 eV. Using a Gaussian with similar widths as we find for Sco X-1 and Cyg X-2 (0.6–0.9 keV), we obtain 3σ upper limits on the equivalent width of less than 10 eV in the 6.4–6.7 keV range for GX 5–1.

We tried to constrain the reflection fraction in our GX 5–1 spectra using `bbrefl` (Ballantyne 2004, using solar Fe abundances), which models the reflection spectrum from a constant-density disk illuminated by a blackbody component. Since the version of the `bbrefl` model that we used includes a blackbody component, the blackbody component that was already part of our model (to account for the boundary layer emission) was removed. In our fits to the HB spectrum, in which we found the boundary layer to have the highest temperature, the ionization parameter, $\log(\xi)$, pegged at its highest allowed value of 3.75. The reflection fraction f_{refl} is very low, with a 3σ upper limit of ~ 0.03 . The boundary layer temperature was 2.41 ± 0.02 keV (compared to 2.51 ± 0.04 keV without the inclusion of the reflection component, see Table 2), while the normalization of the `bbrefl` component had a value of $1.98_{-0.06}^{+2.00} \times 10^{-26}$. Spectra from other parts of the Z track showed similar behavior: very low reflection fractions and $\log(\xi)$ values

Table 3. Spectral-fit parameters for Sco X-1 and Cyg X-2

	Sco X-1 (NB)	Cyg X-2 (Upper NB)
$N_{\text{H}}(10^{21} \text{ atoms cm}^{-2})$	1.5 ^a	2 ^a
kT_{disk} (keV)	1.78±0.02	1.64±0.02
R_{in} (km)	9.73±0.18	18.4±0.6
kT_{bb} (keV)	2.64±0.02	2.37±0.06
R_{bb} (km)	2.94±0.09	3.62±0.15
PL index	3.70±0.05	2.4±0.3
E_{cut} (keV)	—	13±5
E_{Gauss} (keV)	6.60±0.04	6.45±0.09
σ_{Gauss} (keV)	0.61±0.08	0.91±0.10
norm _{Gauss}	$(1.38±0.17) \times 10^{-1}$	$(1.3±2) \times 10^{-2}$
$F_{3-50 \text{ keV}}^b$ ($10^{-8} \text{ erg cm}^{-2} \text{ s}^{-1}$)	19.22±0.03	1.57±0.12
PL Fraction (%)	0.9±0.4	10±3
$L_{1-100 \text{ keV}}$ ($10^{38} \text{ erg s}^{-1}$)	2.445±0.002	3.34±0.17

NOTE—For R_{in} , R_{bb} , and L_{1-100} we assumed distances of 2.8 kpc and 11 kpc for Sco X-1 and Cyg X-2, respectively (Bradshaw et al. 1999; Galloway et al. 2008). For R_{in} we additionally assumed an inclination of 30° for Sco X-1 and 60° for Cyg X-2. For $L_{1-100 \text{ keV}}$ the power-law contribution was only measured between 3 and 100 keV.

^a parameter was fixed

^b Absorbed

close to or pegged at 3.75. For comparison, using the same model for Sco X-1, we found $\log(\xi) = 3.32 \pm 0.07$ and $f_{\text{refl}} = 1.0^{+0.8}_{-0.3}$, while for Cyg X-2 we obtained $\log(\xi) = 3.66^{+0.01}_{-0.03}$ and f_{refl} at its maximum allowed value of 5.0.

4. DISCUSSION

We have analyzed three *NuSTAR* observations of the Cyg-like Z source GX 5–1. Together, these three observations cover almost the entire Z track of the source, from the HB to the dipping FB. The main result from our analysis is the lack of clear disk reflection features in any of the spectra along the Z track of GX 5–1. This is surprising, given the presence of strong and broad Fe K_α lines in *NuSTAR* spectra of many NS-LMXBs (see Table 1), and in particular the Z sources GX 17+2 (Ludlam et al. 2017c), GX 349+2 (Coughenour et al. 2017), Cyg X-2 (Mondal et al. 2018, this work), and Sco X-1 (this work). A broad Fe line has also been reported in *XMM-Newton* spectra of the Z source GX 340+0 (D’Aì et al. 2009; Cackett et al. 2010), a source that is often considered a close twin of GX 5–1. The only two NS-LMXBs without reported reflection features in *NuSTAR* spectra are GS 1826–238 (Chenevez et al. 2016), which had a luminosity of $\sim 0.13 L_{\text{Edd}}$, and Cen X-4

(Chakrabarty et al. 2014), which was observed in quiescence at $3.8 \times 10^{-6} L_{\text{Edd}}$.

Based on a study of broad Fe K_α lines in 10 NS-LMXBs, Cackett et al. (2010) concluded that the boundary layer emission dominates the flux irradiating the inner accretion disk. GX 5–1 shows a hot and strong boundary layer component in our *NuSTAR* spectra, reaching temperatures as high as ~ 2.5 keV on the HB. Our fits also suggest that the inner accretion disk extends close to the neutron star on the HB and NB. Given this combination of parameters one would expect to see Fe K_α reflection features on at least part of the Z track of GX 5–1. In the following we discuss several possible explanations for the absence of reflection features in the X-ray spectra of GX 5–1:

1. As the ionization parameter ξ increases to a few times 10^4 one expects the Fe K_α line to become weakened and broadened as the result of Compton scattering (Ross et al. 1999), making it hard to detect them, even in bright sources. As can be seen from Table 1, GX 5–1 is at the top of the luminosity range of NS-LMXBs observed with *NuSTAR*, although it should be noted that distances to many of the NS-LMXBs are uncertain.

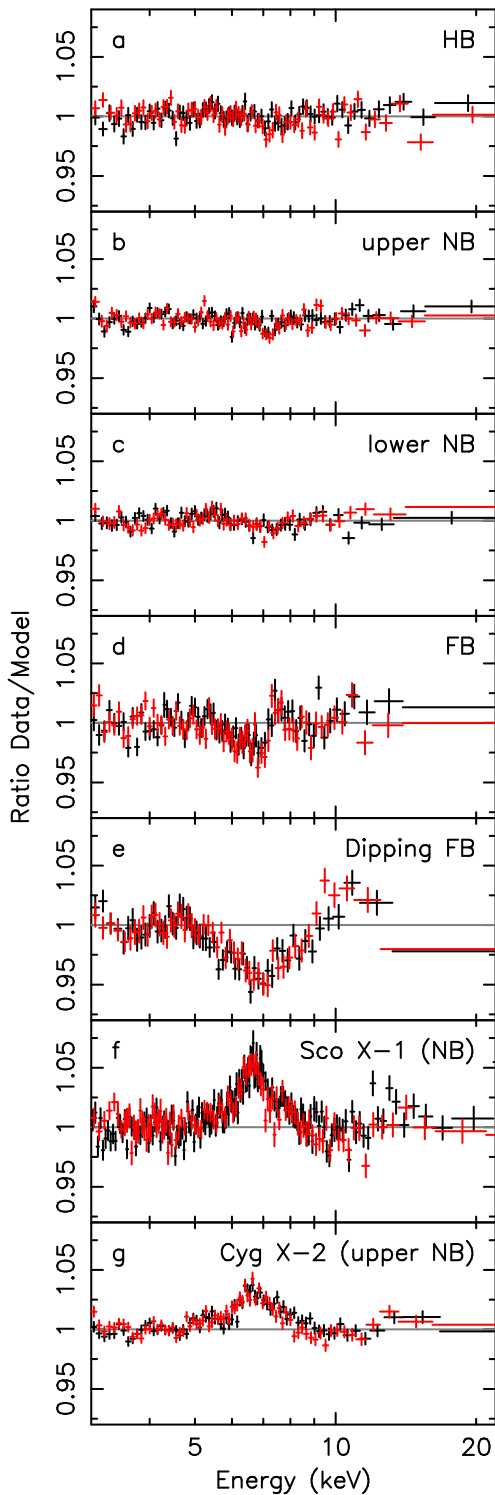


Figure 3. Data-to-model ratios for the spectra from our five HID selections and for archival *NuSTAR* spectra of Sco X-1 (panel (f)) and Cyg X-2 (panel (g)). Data in the 5.0–8.0 keV were initially excluded from the fit, but were reintroduced for the plot. FMPA data are shown in black, FPMB data in red.

Given the high ξ values we measured in Sco X-1

and Cyg X-2, a ξ value close to 10^4 for GX 5–1 might not be unreasonable.

2. The Fe abundance plays an important role in the overall shape of the reflection component, with a low Fe abundance resulting in a weak or absent Fe K_{α} line (Ross et al. 1999). However, the lower limit on the Fe abundance reported by Zeegers et al. (2017), >0.76 , rules out a highly subsolar Fe abundance.
3. The inclination affects the observed shape of Fe K_{α} lines produced in the inner accretion disk, as the result of relativistic effects, leading to very broad lines in the case of nearly edge-on systems (Laor 1991) that might blend in with the continuum components. However, the high viewing angles required for extreme broadening would likely result in observational effects such as periodic absorption dips or eclipses in the light curves (Frank et al. 1987), neither of which are seen in GX 5–1.
4. As the luminosity of NS-LMXBs approaches or exceeds the Eddington luminosity, changes in the accretion geometry are likely to occur, as witnessed by the dramatic changes in the Z tracks of, e.g., XTE J1701–462 and Cir X-1 (Fridriksson et al. 2015). Although the nature of these changes is unknown, it is possible that a combination of changes in the boundary layer and accretion disk result in less efficient illumination of the inner accretion disk at super-Eddington luminosities, causing weaker reflection features. We deem this unlikely, given the presence of strong Fe K_{α} lines in other super-Eddington Z sources.

Given the high luminosity of GX 5–1, we consider high ξ values the most likely explanation for the absence of reflection features in its spectra, although this is not without potential challenges. First, why do GX 340+0, a close twin to GX 5–1, and Cyg X-2, which had a similar luminosity to GX 5–1 in its *NuSTAR* observations, both show broad Fe K_{α} lines, while GX 5–1 does not? A proper luminosity comparison of all Z sources would be required to determine how the luminosity of GX 5–1 truly ranks among the Z sources. This, in turn, requires more accurate distances, inclinations, and spectra measured over a wider energy range. Second, if there are no reflection features from the inner disk because it is too highly ionized, why are they not observed from less ionized regions further out in the disk? The large thickness of the inner accretion disk at super-Eddington luminosities will likely lead to shielding of those parts of the disk, thereby limiting the amount of emission from the

central source that could produce reflection features. Finally, as discussed in White et al. (1988) and Zdziarski et al. (2003) even in the case of a fully ionized disk, the Klein-Nishina process should lead to an observable high-energy break (around a few tens of keV) due to reflection, especially if the illuminating emission extends well beyond that energy. However, since the reflection in high-luminosity NS-LMXBs appears to be dominated by emission originating in the boundary layer (Cackett et al. 2010), a high-energy break in the reflected blackbody emission from the boundary layer might be difficult to detect. Indeed, we do not detect such a break in the spectra of Sco X-1 and Cyg X-2 that we analyzed either; both of these spectra show Fe K_α lines, indicating that reflection is taking place, and both suggest a high-ionization state of the disk ($\xi \sim 3.3 - 3.7$).

The absence of reflection features in GX 5–1 may indicate a link with ultra-luminous X-ray sources (ULXs). We measured 1–100 keV fluxes of $(3.0\text{--}4.3) \times 10^{38} (d_9)^2$ erg s^{−1}, which start to approach the traditionally used lower boundary of ULXs (10^{39} erg s^{−1}). Strong curvature in the 6–8 keV range in *XMM-Newton* spectra of some ULXs has been interpreted as a relativistically broadened Fe K_α line, but *NuSTAR* data have shown that reflection models can be ruled out as an explanation of that feature (Walton et al. 2014; Rana et al. 2015). As far as we are aware, reflection features have not yet been observed in *NuSTAR* spectra of ULXs. Perhaps, as we suggest for GX 5–1, the inner accretion disks in

ULXs are also fully ionized, as the result of their super-Eddington luminosities. In NS-LMXBs the luminosity of GX 5–1 ($\sim 2 L_{\text{Edd}}$) possibly represents a critical value for the presence of reflection features (see Table 1).

The lack of reflection features in the spectra of GX 5–1 means that we could not perform tests of our continuum model by obtaining independent measurements of the inner disk radius. Although the overall decrease in disk and/or boundary layer temperatures from the HB down to the dipping FB is consistent with earlier spectral studies of GX 5–1 (Paizis et al. 2005; Jackson et al. 2009), disk properties, as well as the N_{H} and the power-law index, remain difficult to constrain without coverage below 3 keV. Simultaneous coverage with *NICER* (Gendreau et al. 2016) during future *NuSTAR* observations of Z sources may provide better constraints on the spectral evolution along their Z tracks.

J.H. acknowledges financial support from NASA grant NNX15AV35G. R.L. acknowledges funding through a NASA Earth and Space Sciences Fellowship. We thank Sasha Zeegers for discussions on the Fe abundance and N_{H} values of GX 5–1, and Andrzej Zdziarski for his suggestions about the presence of a possible high-energy break. This research has made use of data and/or software provided by the High Energy Astrophysics Science Archive Research Center, which is a service of the Astrophysics Science Division at NASA/GSFC and the High Energy Astrophysics Division of the Smithsonian Astrophysical Observatory.

REFERENCES

- Arnaud, K. A. 1996, in *Astronomical Society of the Pacific Conference Series*, Vol. 101, ASP Conf. Ser., ed. G. H. Jacoby & J. Barnes, 17
- Ballantyne, D. R. 2004, *MNRAS*, 351, 57
- Bradshaw, C. F., Fomalont, E. B., & Geldzahler, B. J. 1999, *ApJL*, 512, L121
- Cackett, E. M., Miller, J. M., Bhattacharyya, S., et al. 2008, *ApJ*, 674, 415
- Cackett, E. M., Miller, J. M., Ballantyne, D. R., et al. 2010, *ApJ*, 720, 205
- Chakrabarty, D., Tomsick, J. A., Grefenstette, B. W., et al. 2014, *ApJ*, 797, 92
- Chenevez, J., Galloway, D. K., in 't Zand, J. J. M., et al. 2016, *ApJ*, 818, 135
- Christian, D. J., & Swank, J. H. 1997, *ApJS*, 109, 177
- Church, M. J., Halai, G. S., & Bałucińska-Church, M. 2006, *A&A*, 460, 233
- Coughenour, B. M., Cackett, E. M., & Miller, J. M. 2017, ArXiv e-prints, arXiv:1708.01652
- D’Ài, A., Iaria, R., Di Salvo, T., Matt, G., & Robba, N. R. 2009, *ApJL*, 693, L1
- Degenaar, N., Miller, J. M., Chakrabarty, D., et al. 2015, *MNRAS*, 451, L85
- Degenaar, N., Altamirano, D., Parker, M., et al. 2016, *MNRAS*, 461, 4049
- Fabian, A. C., & Ross, R. R. 2010, *SSRv*, 157, 167
- Frank, J., King, A. R., & Lasota, J. . 1987, *A&A*, 178, 137
- Fridriksson, J. K., Homan, J., & Remillard, R. A. 2015, *ApJ*, 809, 52
- Fürst, F., Nowak, M. A., Tomsick, J. A., et al. 2015, *ApJ*, 808, 122
- Galloway, D. K., Muno, M. P., Hartman, J. M., Psaltis, D., & Chakrabarty, D. 2008, *ApJS*, 179, 360

- Gendreau, K. C., Arzoumanian, Z., Adkins, P. W., et al. 2016, in Proc. SPIE, Vol. 9905, Space Telescopes and Instrumentation 2016: Ultraviolet to Gamma Ray, 99051H
- Homan, J., van der Klis, M., Fridriksson, J. K., et al. 2010, ApJ, 719, 201
- Jackson, N. K., Church, M. J., & Bałucińska-Church, M. 2009, A&A, 494, 1059
- King, A. L., Tomsick, J. A., Miller, J. M., et al. 2016, ApJL, 819, L29
- Kuulkers, E., van der Klis, M., Oosterbroek, T., et al. 1994, A&A, 289, 795
- Laor, A. 1991, ApJ, 376, 90
- Lin, D., Remillard, R. A., & Homan, J. 2009, ApJ, 696, 1257
- Ludlam, R. M., Miller, J. M., Cackett, E. M., Degenaar, N., & Bostrom, A. C. 2017a, ApJ, 838, 79
- Ludlam, R. M., Miller, J. M., Degenaar, N., et al. 2017b, ApJ, 847, 135
- Ludlam, R. M., Miller, J. M., Cackett, E. M., et al. 2016, ApJ, 824, 37
- Ludlam, R. M., Miller, J. M., Bachetti, M., et al. 2017c, ApJ, 836, 140
- Matranga, M., Di Salvo, T., Iaria, R., et al. 2017, A&A, 600, A24
- Miller, J. M., Parker, M. L., Fuerst, F., et al. 2013, ApJL, 779, L2
- Mondal, A. S., Dewangan, G. C., Pahari, M., & Raychaudhuri, B. 2018, MNRAS, 474, 2064
- Mondal, A. S., Pahari, M., Dewangan, G. C., Misra, R., & Raychaudhuri, B. 2017, MNRAS, 466, 4991
- Paizis, A., Ebisawa, K., Tikkanen, T., et al. 2005, A&A, 443, 599
- Rana, V., Harrison, F. A., Bachetti, M., et al. 2015, ApJ, 799, 121
- Reynolds, C. S. 2014, SSRv, 183, 277
- Ross, R. R., Fabian, A. C., & Young, A. J. 1999, MNRAS, 306, 461
- Sleator, C. C., Tomsick, J. A., King, A. L., et al. 2016, ApJ, 827, 134
- Titarchuk, L., Seifina, E., & Shrader, C. 2014, ApJ, 789, 98
- Verner, D. A., Ferland, G. J., Korista, K. T., & Yakovlev, D. G. 1996, ApJ, 465, 487
- Walton, D. J., Harrison, F. A., Grefenstette, B. W., et al. 2014, ApJ, 793, 21
- Wang, Y., Méndez, M., Sanna, A., Altamirano, D., & Belloni, T. M. 2017, MNRAS, 468, 2256
- White, T. R., Lightman, A. P., & Zdziarski, A. A. 1988, ApJ, 331, 939
- Wilms, J., Allen, A., & McCray, R. 2000, ApJ, 542, 914
- Zdziarski, A. A., Johnson, W. N., & Magdziarz, P. 1996, MNRAS, 283, 193
- Zdziarski, A. A., Lubiński, P., Gilfanov, M., & Revnivtsev, M. 2003, MNRAS, 342, 355
- Zeegers, S. T., Costantini, E., de Vries, C. P., et al. 2017, A&A, 599, A117
- Życki, P. T., Done, C., & Smith, D. A. 1999, MNRAS, 309, 561